Exciplex fluorescence emission from simple organic intramolecular constructs in non-polar and highly polar media as model systems for DNA-assembled exciplex detectors†

Elena V. Bichenkova,* Ali R. Sardarian, Amanda N. Wilton, Pascal Bonnet, Richard A. Bryce and Kenneth T. Douglas

Received 17th August 2005, Accepted 17th November 2005
First published as an Advance Article on the web 8th December 2005
DOI: 10.1039/b511707k

Organic intramolecular exciplexes, *N*-(4-dimethylaminobenzyl)-*N*-(1-pyrenemethyl)amine (**1**) and *N*′-4-dimethylaminonaphthyl-*N*-(1-pyrenemethyl)amine (**2**), were used as model systems to reveal major factors affecting their exciplex fluorescence, and thus lay the basis for developing emissive target-assembled exciplexes for DNA-mounted systems in solution. These models with an aromatic pyrenyl hydrocarbon moiety as an electron acceptor appropriately connected to an aromatic dimethylamino electron donor component (*N*,*N*-dimethylaminophenyl or *N*,*N*-dimethylaminonaphthyl) showed strong intramolecular exciplex emission in both non-polar and highly polar solvents. The effect of dielectric constant on the maximum wavelength for exciplex emission was studied, and emission was observed for **1** and **2** over the full range of solvent from non-polar hydrocarbons up to *N*-methylformamide with a dielectric constant of 182. Quantum yields were determined for these intramolecular exciplexes in a range of solvents relative to that for Hoechst 33258. Conformational analysis of **1** was performed both computationally and *via* qualitative 2D NMR using ^{1}H-NOESY experiments. The results obtained indicated the contribution of pre-folded conformation(s) to the ground state of **1** conducive to exciplex emission. This research provides the initial background for design of self-assembled, DNA-mounted exciplexes and underpins further development of exciplex-based hybridisation bioassays.

Introduction

We have recently introduced the first oligonucleotide-based chemical constructs that can self-assemble at their complementary DNA target (Scheme 1a) to produce emissive exciplexes with their characteristic long-wavelength fluorescence.[1,2] This method can efficiently detect single mutations and, thus, represents a new type of technique for genotyping and gene expression profiling. This approach, which introduced the means to assemble emissive exciplexes for DNA detection systems, opens routes to a novel class of *in vitro* molecular diagnostic techniques, providing a step-increase in bio-specificity, reliability, accuracy and quality assurance. Whilst a similar split-probe approach has been reported for excimer-based detectors,[3–7] the solvent dependence of exciplexes presented us with a significant problem to overcome for DNA duplexes, which primarily exist in highly polar solvent media.

Despite this dilemma, exciplex-based approaches offer more property diversity than excimers (*e.g.*, freedom in selection of exci-partners, variability in excitation and emission λ_{max}, *etc.*) and thence in potential applications.

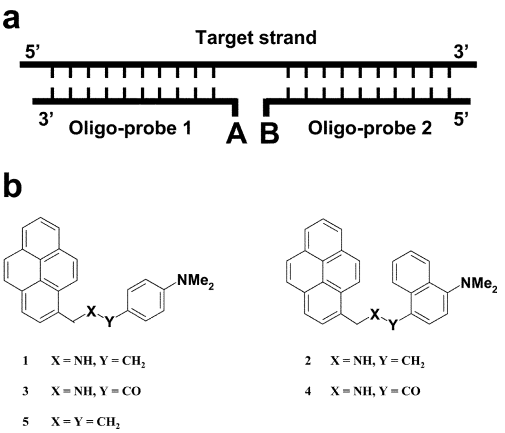

Scheme 1 (a) Schematic presentation of split-probe approach showing self-assembly of exciplex components (**A** and **B**) induced by hybridisation of oligo-probes with complementary nucleic acid target. (b) Chemical structures of model intramolecular exciplex systems of the present study.

Exciplex emission is generally known to be strongly quenched as the solvent becomes more polar, in contrast to excimers which are much less sensitive to their solvent polarity. Intermolecular organic exciplexes do not usually emit even in solvents as polar as acetonitrile.[8–11] In contrast, several intramolecular exciplexes

Wolfson Centre for Structure-Based Rational Design of Molecular Diagnostics, School of Pharmacy and Pharmaceutical Sciences, University of Manchester, Manchester, UK M13 9PL. E-mail: Elena.Bichenkova@manchester.ac.uk; Fax: 44 (0)161 275 2481; Tel: 44 (0)161 275 8359

† Abbreviations used: DCM, dichloromethane; DMSO, dimethyl sulfoxide; DMA, *N*,*N*-dimethylaminophenyl; DEA, *N*,*N*-diethylaniline; DMN, *N*,*N*-dimethylaminonaphthyl; EGDE, ethyleneglycol dimethyl ether; LES, locally excited state; Pyr, pyrene; SM, small molecule; THF, tetrahydrofuran.

exhibit exciplex emission in solvents up to the polarity of acetonitrile.[12–21] This behavioural shift has been ascribed to a change in structure for exciplexes going from compact in nonpolar solvents to loose in polar solvents.[20,22] For strongly interacting exciplex partners, such as aromatic hydrocarbons with dialkylanilines, the exciplex arises from a partial charge-transferred state, which is sufficiently stable in nonpolar solvents to fluoresce. Increased solvent polarity preferentially solvates and stabilises charge separation and at a dielectric constant of approximately 14 the pyrene:diethylaniline pair has an exciplex absorption spectrum identical with the ion pair, pyrene^{-}:$PhNEt_2^{+}$.[23] Intramolecular exciplexes have recently been discovered which emit in solvents as polar as DMSO, propylene carbonate, or even 20% aqueous acetonitrile.[24] Intermolecular exciplex luminescence in polar: nonpolar solvent mixtures (such as DMSO–benzene,[25] water–THF or water–dioxane[25]) can be enhanced by magnetic fields.

To approach the problem of weak exciplex emission at the DNA level we studied the influence of various factors (*i.e.*, solvent polarity, composition of exci-partners and structural aspects of ground-state conformations) on exciplex formation by means of simple intramolecular model systems (Scheme 1b, **1**–**4**). This work provides examples of novel intramolecular exciplexes (**1** and **2**) with strong exciplex emission in many solvents, even with dielectric constants up to 182. The observations obtained in this work provided the initial background for DNA-mounted exciplexes and underpin further development of exciplex-based nucleic acid hybridisation assays. For oligo-mounted DNA/RNA exciplex systems[1,2] we discovered specific co-solvents (best was trifluoroethanol), which allow massive enhancement of the exciplex signal. By changing the hydrophobicity of the environment, this co-solvent regulates the excited-state attraction of the exci-partners, influences DNA structure itself,[26] and affects competitive binding of exci-partners to the duplex architecture.[27,28]

Results

Evidence for intramolecular exciplex emission

Fig. 1 compares the emission spectra of **1** and **2** in toluene with the emission spectra of free pyrene under identical conditions (1×10^{-5} M, 20 °C). All these spectra show the characteristic emission bands of the LES of pyrene between 350 and 450 nm, the emission λ_{max} being 373 nm for free pyrene and 377 nm for both **1** and **2**. However, the emission intensity of the LES is significantly less for both **1** and **2** compared with free pyrene, and for each a new intense band is observed at longer wavelength, between 450 and 650 nm. In the case of **1** this band, with an emission λ_{max} of 498 nm, is attributed to intramolecular exciplex formation between the pyrenyl and 4-*N*,*N*′-dimethylaminoanilino moieties. For **2**, the corresponding exciplex between the pyrenyl and *N*′-4-dimethylaminonaphthyl partners is observed at a longer wavelength (emission λ_{max} 522 nm). This new emission band cannot be attributed to intermolecular excimer formation between pyrenyl moieties from two molecules of either **1** or **2**, as there was no excimer formation seen for pyrene at the same concentration under identical conditions (Fig. 1). Moreover, experiments involving mixing the free exci-partners (unlinked pyrene and DMA) under identical conditions to those used for the exciplex studies, did not show any emission band that could be ascribed to intermolecular exciplex formation, until the concentration of the DMA was increased to at least 100- to 1000-fold (*i.e.*, at 1×10^{-3} to 1×10^{-2} M) with respect to pyrene.

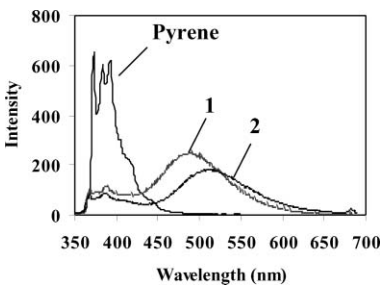

Fig. 1 Emission spectra of pyrene, **1** and **2** in toluene, recorded at 1×10^{-5} M and 20 °C with excitation wavelengths of 337, 345 and 346 nm, respectively.

Solvent influence on excitation and emission spectra

Emission and excitation properties of **1** and **2** were analyzed in a broad range of organic solvents with dielectric constants ranging from 2.02 to 181.6. The values of λ_{max} for emission and excitation of **1** and **2**, along with extinction coefficients and relative quantum yields, are summarised in Table 1 and 2, respectively. Fig. 2 and 3 show emission spectra of **1** and **2**, respectively, in a number of representative organic solvents covering dielectric constants from 2.02 to 40.25.

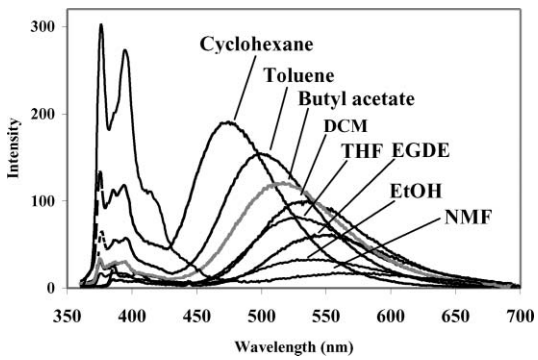

Fig. 2 Emission spectra at 20 °C of **1** (1×10^{-5} M) in various organic solvents. Excitation wavelengths for both locally excited state and exciplex band, optimised for each solvent, are given in Table 1.

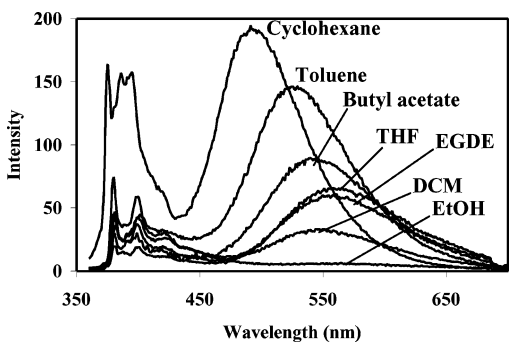

Fig. 3 Emission spectra of **2** (1×10^{-5} M) in various organic solvents at 20 °C. Excitation wavelengths for both locally excited state and exciplex band, optimised for each solvent, are given in Table 2.

Table 1 Fluorescence and absorption characteristics of **1** in organic solvents. Excitation wavelength was optimised for each solvent, and normally corresponded to the λ_{max} of excitation of the pyrene monomer (λ^{M}_{max}). For certain solvents, relative quantum yields $\Phi_{(I)}$ of the exciplex emission band of **1** as well as extinction coefficients ε were determined. Figures in brackets indicate wavelengths at which ε values were determined

Solvent	Dielectric constant	Monomer excitation λ^{M}_{max}/nm[a]	Exciplex excitation λ^{E}_{max}/nm[b]	Monomer Emission $^{M}_{max}$/nm[a]	Exciplex Emission λ^{E}_{max}/nm[b]	AUC^{M}[c]	AUC^{E}[c]	Extinction coefficient, ε/M^{-1} cm^{-1}	Relative quantum yield, $\Phi_{(I)}$
Cyclohexane	2.02	342	342	377	475	0.31	0.69	—	—
Hexyl ether	2.12	344	344	377	490	0.29	0.71	—	—
1,4-Dioxane	2.21	342	343	376	515	0.11	0.89	—	—
Toluene	2.23	345	345	377	498	0.23	0.77	42500 ± 2500 (345 nm)	0.0321 ± 0.0011
1-Octanol	3.40	343	343	375	524	0.28	0.72	—	—
Diethyl ether	4.24	341	341	375	508	0.11	0.89	49500 ± 2500 (341 nm)	0.0190 ± 0.0007
Chloroform	4.71	344	344	376	512	0.14	0.86	—	—
Butyl acetate	4.99	342	342	375	520	0.15	0.85	—	—
Chlorobenzene	5.70	346	346	376	517	0.07	0.93	—	—
Ethyl acetate	5.99	341	341	375	528	0.35	0.65	44250 ± 750 (342 nm)	0.0137 ± 0.0008
THF	7.43	343	343	376	530	0.20	0.80	49250 ± 1750 (343 nm)	0.0161 ± 0.0009
DCM	9.83	344	344	376	530	0.11	0.89	—	—
Dichlorobenzene	9.99	347	347	377	524	0.06	0.94	—	—
Isopropanol	19.264	342	342	375	534	0.16	0.84	—	—
Acetone	20.49	341	341	376	552	0.14	0.86		
Ethanol	24.85	340	340	375	530	0.83	0.17	55500 ± 1500 (342 nm)	0.0076 ± 0.0004
TFE	26.73	339	339	374	Negligible	1.00	0.00	—	—
Acetonitrile	35.68	341	341	376	558	0.94	0.06	—	—
DMF	37.22	338	344	377	567	0.74	0.26	—	—
EGDE	40.245	343	343	375	538	0.10	0.90	47500 ± 2500 (344 nm)	0.0138 ± 0.0005
DMSO	46.83	344	338	376	558	0.93	0.07	—	—
Formamide	108.94	343	343	376	Negligible	1.00	0.00	—	—
Methyl formamide	181.56	342	342	377	571	0. 91	0.09	—	—

[a] λ^{M}_{max} refers to monomer excitation or monomer emission. [b] λ^{E}_{max} refers to exciplex excitation or exciplex emission. [c] AUC^{M} and AUC^{E} are the fractional areas under the corrected emission curve for monomer and exciplex fluorescence band, respectively, normalised relative to the total integral emission of **1**, AUC$^{\Sigma}$, where AUC$^{\Sigma}$ = AUC^{M} + AUC^{E}, and AUC$^{\Sigma}$ = 1.

Table 2 Fluorescence and absorption characteristics of **2** in organic solvents. Excitation wavelength was optimised for each solvent, and normally corresponded to the λ_{max} of excitation of the pyrene monomer (λ^{M}_{max}). For certain solvents, relative quantum yields $\Phi_{(2)}$ of the exciplex emission band of **2** as well as extinction coefficients ε were determined. Figures in brackets indicate wavelengths at which ε values were determined

Solvent	Dielectric constant	Excitation λ^{M}_{max}/nm[a]	Excitation $^{E}_{max}$/nm[b]	Emission λ^{M}_{max}/nm[a]	Emission $^{E}_{max}$/nm[b]	AUC^{M}[c]	AUC^{E}[c]	Extinction coefficient, ε/M^{-1} cm^{-1}	Relative quantum yield, $\Phi_{(2)}$
Cyclohexane	2.02	342	342	375	493	0.36	0.64	—	—
Hexyl ether	2.12	342	342	376	497	0.40	0.60	—	—
1,4-Dioxane	2.21	343	344	376	534	0.28	0.72	—	—
Toluene	2.23	346	346	377	522	0.29	0.71	42000 ± 400 (346 nm)	0.0219 ± 0.0024
1-Octanol	3.40	343	343	375	542	0.58	0.42	—	—
Diethyl ether	4.24	341	341	375	522	0.13	0.87	—	0.0146 ± 0.0011
Chloroform	4.71	345	345	377	529	0.44	0.56	—	—
Butyl acetate	4.99	342	342	375	536	0.17	0.83	—	—
Chlorobenzene	5.70	346	346	377	534	0.19	0.81	—	—
Ethyl acetate	5.99	342	342	375	554	0.39	0.61	43450 ± 550 (342 nm)	0.0121 ± 0.0012
THF	7.43	343	343	376	555	0.25	0.75	50233 ± 2500 (343 nm)	0.0126 ± 0.0016
DCM	9.83	345	345	376	542	0.50	0.50	—	—
Dichlorobenzene	9.99	347	347	377	538	0.31	0.69	—	—
Isopropanol	19.264	341	342	375	553	0.46	0.54	—	—
Acetone	20.49	341	342	375	581	0.70	0.30	—	—
Ethanol	24.85	340	340	375	555	0.86	0.14	54200 ± 2500 (342 nm)	—
TFE	26.73	338	—	374	Negligible (tail)	1.00	0.00	—	—
Acetonitrile	35.68	340	342	375	586	0.74	0.26	—	—
DMF	37.22	338	338	375	582	0.89	0.11	—	—
EGDE	40.245	343	343	375	557	0.31	0.69	45880 ± 2280 (343 nm)	0.0153 ± 0.0005
DMSO	46.83	344	—	376	Negligible	1.00	0.00	—	—
Formamide	108.94	341	—	376	Negligible	1.00	0.00	—	—
Methyl formamide	181.56	343	—	376	ND	1.0	0.00	—	—

[a] λ^{M}_{max} refers to monomer excitation or monomer emission. [b] λ^{E}_{max} refers to exciplex excitation or exciplex emission. [c] AUC^{M} and AUC^{E} are the fractional areas under the corrected emission curve for monomer and exciplex fluorescence band, respectively, normalised relative to the total integral emission of **2**, AUC$^{\Sigma}$, where AUC$^{\Sigma}$ = AUC^{M} + AUC^{E}, and AUC$^{\Sigma}$ = 1.

The data in Tables 1 and 2 show that solvent polarity has very little effect on the emission λ_{max} of the LES of the pyrenyl partner for either **1** or **2**, the value of which normally ranges from 374 to 377 nm. In contrast, exciplex emission shows a much greater dependence on solvent dielectric constant, with emission λ_{max} varying over a range of nearly 100 nm. The λ_{max} values for emission of **1** range from 475 nm (cyclohexane, $\varepsilon = 2.02$) to 571 nm (*N*-methylformamide, $\varepsilon = 181.56$); for **2** the range is from 493 nm (cyclohexane, $\varepsilon = 2.02$) to 586 nm (acetonitrile $\varepsilon = 35.68$). These experimental observations are consistent with the extensive literature showing that solvent polarity is crucial to the properties of exciplexes, whilst the wavelength of excimer emission is relatively solvent independent.[29] However, it is novel that reasonably strong exciplex emission from such constructs can be readily detected with standard spectrophotofluorimetry instrumentation for very high dielectric solvents as shown in Table 1.

There appears to be a correlation between the dielectric constant of the solvent, and the frequency corresponding to λ_{max} of the exciplex emission band in that solvent (see Tables 1 and 2). At lower dielectric constant values ($2.02 \leq \varepsilon \leq 10$), there is an almost linear relationship between the two parameters, whilst at higher values ($\varepsilon \geq 10$) this relationship is less well defined and tends to level off. Clearly, in addition to solvent dielectric constant other physicochemical factors (*e.g.* refractive index) affect the value of λ_{max} for exciplex emission.

Another important property of exciplex emission is that this solvent-induced bathochromic shift in exciplex λ_{max} is normally accompanied by a decrease in intensity of exciplex emission (see Fig. 2 and 3). Such exciplex quenching in intramolecular exciplexes is most commonly effectively total once solvent polarities greater than that of acetonitrile are reached. Compounds **1** and **2** provide cases for which exciplex emission is clearly possible even in extremely high dielectric constant media such as *N*-methylformamide for **1**.

Influence of the exciplex donor and acceptor partners on exciplex emission

Comparison of the emission spectra of **1** and **2** in a variety of organic solvents (Fig. 4), allows the evaluation of the influence of different partners on exciplex emission properties. As a rule the exciplex from **2** emits at a longer wavelength than that of **1**, and generally shows lower emission intensity of both LES and exciplex bands (Table 1 and 2).

Relative quantum yields

The relative quantum yields of the exciplex bands of **1** and **2** were determined under identical conditions in a range of organic solvents covering dielectric constant values from 2.02 to 40.25 and are given in Table 1 and 2, respectively. For both **1** and **2** the highest quantum yield was found in toluene. There was a general tendency for a decrease of quantum yield with increasing solvent polarity, although some exceptions were observed, especially in the case of **2**, indicating the influence of other physicochemical factors on quantum yields. In each solvent studied, the relative quantum yield of **1** was generally 1.13 to 1.5 times higher than that of **2**, except for the case of EGDE, in which opposite result was obtained, but the difference between two values was small.

Intermolecular exciplexes

Studies were carried out to assess the influence of the 4-substituted dimethylaniline on emission maximum of the intermolecular exciplex formed by pyrenemethylamine as a free base (1×10^{-5} M) and the respective dimethylanilino derivative (1×10^{-2} M). The emission maxima (λ_{max}) of the exciplex band in a number of solvents are summarised in Table 3 for unsubstituted dimethylaniline, 4-(dimethylamino)phenylacetic acid, 4-(dimethylamino)benzylamine, 4,4-*bis*(dimethylamino)-benzophenone, and for **1** for comparison. With the following

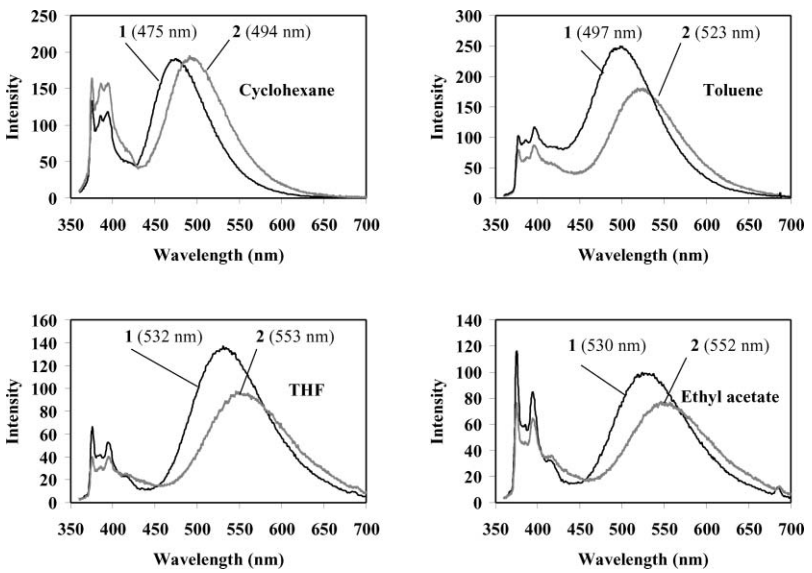

Fig. 4 Comparison of emission spectra at 20 °C of **1** and **2** (at 1×10^{-5} M) in various solvents.

Table 3 Emission data (λ_{max}, nm) for some intermolecular exciplexes formed by pyrenemethylamine (1×10^{-5} M, as free base) and various dimethylanilines (1×10^{-2} M). Exciplex emission data for **1** are presented for comparison (in bold)

		Exciplex emission (λ_{max})/nm			
		Solvent			
Exciplex type (inter- or intramolecular)	Donor partner	Toluene	THF	DCM	EGDE
Intra (**1**)	**DMA**	**498**	**530**	**530**	**538**
Inter	DMA	467	501	495	515
Inter	4-(Dimethylamino)phenylacetic acid	482	503	N/A	N/A
Inter	4-(Dimethylamino)benzylamine	490	502	N/A	N/A
Inter	4,4-Bis(dimethylamino)benzophenone	492	522	N/A	N/A

substituted derivatives the exciplex emission was quenched: 4-(dimethylamino)benzaldehyde, 4-(dimethylamino)benzoic acid and 4,4-*bis*(dimethylamino)benzophenone.

Computational conformational analysis

For insight into the molecular level behaviour of **1** in its ground state as a function of solvent dielectric, conformational analysis was performed using a Monte Carlo/force field search strategy. The effect of low dielectric was simulated using a chloroform solvent model ($\varepsilon = 5$). For a high dielectric environment, the GB/SA parameters for water were adopted ($\varepsilon = 80$). We note that this solvent model may be more representative of high dielectric aprotic solvents as considered in our experiments here, due the absence of explicit first solvation shell effects in the GB model. The lowest energy conformation identified in both solvents was an open, extended structure (**1a** in Fig. 5, Table 4), with a donor–acceptor ring centroid distance of 8.36 Å at high ε and at low ε (Table 4). The open conformation is also illustrated by a donor ring centroid-linker–nitrogen-acceptor ring centroid angle of around 142° (Table 4). A distinct twisted conformation (**1b**) was also identified from the MC/MM search as lying within 0.3 kcal mol^{-1} of **1a** at high ε, and 0.8 kcal mol^{-1} at low ε (Table 4, Fig. 5). This highlights the flexible nature of the molecule around the linker torsions. An interesting feature of this conformation is the apparent stabilisation by a C–H$\cdots\pi$ interaction, indicative of a non-classical hydrogen bond; the distance of the centroid of the *N*,*N*-dimethylaminophenyl ring to the nearest pyrene ring hydrogen is 3.85 Å at high ε and 4.17 Å at low ε.

Table 4 Total energy difference of conformations of **1** (kcal mol^{-1}) with respect to global minimum conformation **1a** (ΔE_{tot}), calculated using the MMFF94s force field and the GB/SA solvent model. Electrostatic (elec), van der Waals (vdw), internal bonded (int) and solvation (solv) contributions in presence of high dielectric solvent (low dielectric solvent in parentheses) also given. Distance between donor and acceptor ring centroids (*R*) in Ångstroms and donor centroid–*N*-acceptor centroid angle (θ) in degrees

	Conformation **1a**	Conformation **1b**	Conformation **1c**
ΔE_{tot}	—	0.3 (0.8)	2.7 (5.7)
ΔE_{vdw}	—	0.2 (0.2)	−2.7 (−1.8)
ΔE_{elec}	—	−0.5 (−0.2)	3.6 (3.5)
ΔG_{solv}	—	0.4 (0.6)	−0.8 (1.5)
ΔE_{int}	—	0.2 (0.2)	2.4 (2.5)
R	8.36 (8.36)	7.36 (7.63)	4.59 (5.06)
θ	142.5 (141.9)	112.2 (119.5)	60.9 (67.7)

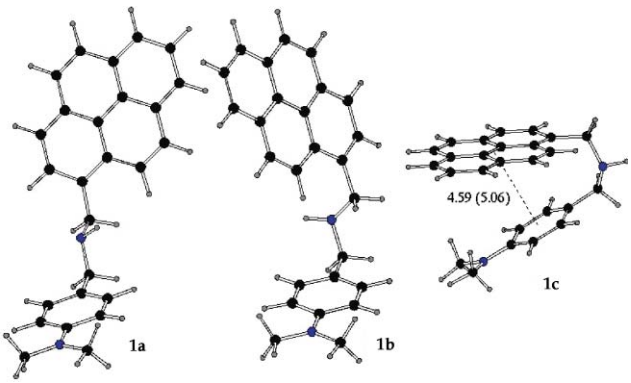

Fig. 5 Three putative, minimum energy conformations of **1** calculated from conformational analysis using the MMFF forcefield in GB/SA solvent (geometric parameters in Table 4). Intercentroid distance is given for conformation **1c** in Å, and value in chloroform in parentheses.

Finally, a higher energy conformation **1c** was identified, with a near-parallel orientation of donor and acceptor groups (Fig. 5). This folded conformation is characterized by intercentroid distances of 4.59 and 5.06 Å in high and low dielectric solvent, respectively (Table 4), smaller than in **1a** or **1b**. As **1c** is predicted to be 2.7 kcal mol^{-1} higher in energy than **1a**, a small fraction of **1c** (1%) may exist at ambient temperatures in high dielectric media. Due to stacking between donor and acceptor π-systems, the folding of conformation **1c** leads to stronger intrasolute van der Waals interactions by 2.7 kcal mol^{-1}, and an improved solvation energy of 0.8 kcal mol^{-1} (Table 4). However, the conformation is strained, with a higher internal (bonded) energy of 2.4 kcal mol^{-1} and less favourable electrostatics than the extended conformation **1a** by 3.6 kcal mol^{-1}. In low dielectric media, the energy difference between **1a** and **1c** is substantially higher, at 5.7 kcal mol^{-1}, indicating that a negligible amount of conformation **1c** would be present at equilibrium (although we note that here the calculated solute contributions are formally potential energies). Considering energetic contributions to stability of **1c** in $CHCl_3$, the total energy difference of 5.7 kcal mol^{-1} is comprised of favourable van der Waals and unfavourable electrostatics and internal energy contributions (Table 4). The solvation component here reverses sign in the lower dielectric medium, failing to stabilise the folded conformation, and it is this term that appears principally responsible for the decreased predicted fraction of folded **1c** at low dielectric. Formation of extended conformation **1a** reduces the electrostatic repulsion (by 3.5 kcal mol^{-1}) as compared with folded conformation **1c**. Therefore, in both low and high dielectric

media, the dominant predicted conformation is an extended, gauche-like structure of the exciplex. However, a folded form of the exciplex, in which HOMO–LUMO overlap of the exci-partner pair would be possible, is calculated to be more accessible at higher dielectric, although still only fractionally populated. Nevertheless, preorganization of the ground state exci-partner pair into a folded state is not requisite for exciplex fluorescence, as excitation can lead to changes in charge distribution and energetics of formation of a folded exciplex conformation subsequently.

Qualitative NMR spectroscopic analysis of ground-state conformation of 1

Proton signal assignment of **1** was performed using 1D ^{1}H NMR and NOESY spectra recorded in $CDCl_3$. The results of proton assignments of **1** are presented in the Experimental section and indicated on Fig. 6.

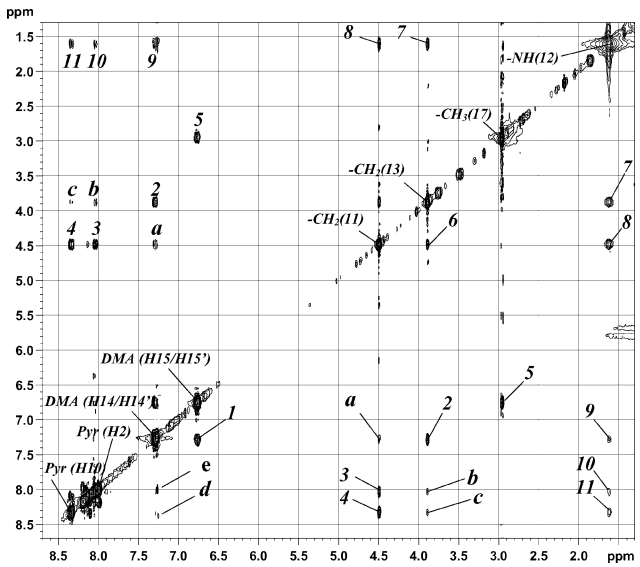

Fig. 6 Expanded region of the ^{1}H NOESY spectrum (300 MHz) of **1** in $CDCl_3$ at 17 °C. The spectrum was recorded with 1.0 s mixing time and a recovery delay of 2.0 s. The sample concentration was 15 mM. The assignments of pyrenyl, DMA and linker protons are shown by diagonal cross-peak labelling. Off-diagonal cross-peaks labelled by figures show some NOE-interactions between closely located protons within the pyrene moiety and within the DMA moiety: ***1***-DMA(H14/14′)–DMA(H15/15′), ***2***: DMA(H14/14′)–CH_2(13), ***3***: Pyr(H2)–CH_2(11), ***4***: Pyr(H10)–CH_2(11), ***5***: DMA(H15/15′)–N–CH_3(17), ***6***: CH_2(11)–CH_2(13), ***7***: CH_2(13)–NH(12), ***8***: CH_2(11)–NH(12), ***9***: DMA(H14/14′)–NH(12), ***10***: Pyr(H2)–NH(12), ***11***: Pyr(H10)–NH(12). Cross-peaks labelled by characters indicate inter-partner interactions between the pyrenyl and DMA moieties: ***a***: DMA(H14/14′)–CH_2(11), ***b***:-Pyr(H2)–CH_2(13); ***c***:-Pyr(H10)–CH_2(13); ***d***:-DMA (H14/H14′)–Pyr(H10), ***e***: DMA (H14/H14′)–Pyr(H2).

Analysis of NOESY spectrum (Fig. 6) revealed the expected positive NOE-interactions between closely located protons within the DMA moiety (*i.e.* DMA(H14/14′)-DMA(H15/15′), cross-peak ***1***; DMA(H14/14′)–CH_2(13), cross-peak ***2***; DMA(H15/15′)–N–CH_3(17), cross-peak ***5***; CH_2(11)–CH_2(13), cross-peak *6*) and within the pyrene moiety (Pyr(H2)–CH_2(11), cross-peak ***3***; Pyr(H10)–CH_2(11), cross-peak ***4***; Pyr(H2)–Pyr(H3), Pyr(H4)–Pyr(H5), Pyr(H6)–Pyr(H7), Pyr(H7)–Pyr(H8) and Pyr(H9)–Pyr(H10), diagonal-adjacent cross-peaks in the 7.9–8.2 ppm area). The assignment of the individual pyrene protons Pyr (H3)–Pyr (H9) was impossible due to extensive overlapping of these signals in the aromatic area of 7.9–8.2 ppm and due to close location of the respective cross-signals to the diagonal in the NOESY spectrum. However, signals Pyr (H2) and Pyr (H10) were assigned unambiguously *via* their interactions with CH_2(11) protons of the linker (cross-peaks ***3*** and ***4***, respectively, Fig. 6). Discrimination between Pyr (H10) and Pyr (H2) was done on the basis of the COSY spectrum of **1** (not shown) recorded in $CDCl_3$. The cross-peak with coordinates (7.99–4.49) ppm was attributed to the interaction between the Pyr(H2) and CH_2(11) groups. Interactions between NH (12) proton and methylene protons CH_2(13) and CH_2(11) were observed as a broad, intensive negative cross-peaks *7* and ***8***, respectively, presumably due to extensive exchange of the NH proton.

In addition a number of H–H contacts that are attributed to inter-partner interactions between the pyrenyl and DMA moieties were detected as positive cross peaks with intensities corresponding to medium or weak through-space H–H interactions in **1** (shown by dashed arrows on Scheme 2). These cross-peaks labelled by symbols ***a***, ***b***, ***c***, ***d*** and ***e*** (Fig. 6) correspond to DMA(H14/14′)–CH_2(11), Pyr(H2)–CH_2(13); Pyr(H10)–CH_2(13), DMA (H14/H14′)–Pyr(H10) and DMA (H14/H14′)–Pyr(H2) interactions, respectively. Also, long-distance, through-space interactions of NH(12) proton with the DMA(H14/H14′), Pyr (H2) and Pyr (H10) protons are observed as medium-intensity cross-peaks ***9***, ***10*** and ***11***, respectively. All NOE cross-peaks have opposite phase to the diagonal, indicating their origin from positive NOE enhancement, as expected for a molecule of this size.[30]

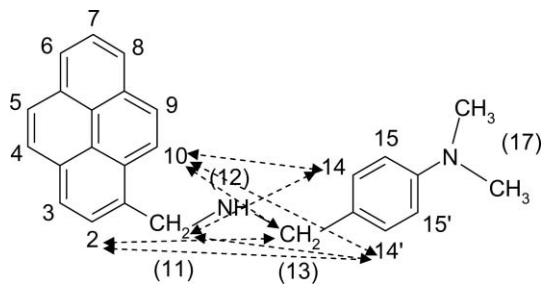

Scheme 2 Numbering of protons of **1** along with some through-space NOE-interactions detected in the NOESY spectrum of **1** (Fig. 6).

Correlation between NMR and molecular modelling data

Molecular modelling calculations disclosed the contribution of two major conformers (**1a** and **1b**) and one minor (**1c**) conformer of **1**, (Fig. 5) with the relative populations 62 : 37 : 1 in water and 80 : 20 : 0 in chloroform at 17 °C. Table 5 represents some proton–proton distances calculated for conformers **1a**, **1b** and **1c** in chloroform along with the respective relative intensities of cross-peaks, observed in the ^{1}H NOESY spectrum recorded in deuteriated chloroform.

It can be seen that distances calculated for conformer **1a** (the lowest energy structure) entirely satisfy experimental NOE observations suggesting that this structure could represent the average conformation of **1** in solution. Although the majority

Table 5 Some proton–proton distances calculated for conformers **1a**, **1b** and **1c** in deuteriated chloroform (calculated population, *p*, at 17 °C) along with the respective relative intensities of cross-peaks, observed in the ^{1}H NOESY spectrum. Intramolecular contacts shown in bold refer to the interactions between the pyrene and DMA partners. The greatest discrepancies between NMR and computational data are shown in bold parentheses

	Interproton distance (Å)				
Intramolecular contacts	**1a** conformer ($p = 80\%$)	**1b** conformer ($p = 20\%$)	**1c** conformer ($p = 0\%$)	Cross-peak assignment (**symbol**/coordinate, ppm)	Relative[b] intensity of observed NOESY cross-peak
Pyr(H2)–CH_2(11)[a]	2.95	2.94	2.84	**3** (8.03–4.48)	s/m
Pyr(H10)–CH_2(11)[a]	2.92	2.92	3.03	**4** (8.32–4.48)	s/m
CH_2(11)[a]–CH_2(13)[a]	2.44	2.97	3.20	**6** (4.48–3.38)	s
DMA(H14/H14′)[a]–CH_2(13)[a]	2.13	2.15	2.13	**2** (7.28–3.88)	s
DMA(H15/15′)–DMA(H14/14′)[a]	2.42	2.42	2.42	**1** (7.28–6.75)	s
DMA(H15/H15′)[a]–N–CH_3(17)	3.05	3.05	3.05	**5** (6.75–2.95)	s
DMA(H14/H14′)–CH_2(11)[a]	**4.16**	**3.21**	**3.95**	**a** (7.28–4.48)	**m**
Pyr(H2)–CH_2(13)[a]	**4.62**	**4.60**	**4.00**	**b** (8.03–3.88)	**w**
Pyr(H10)–CH_2(13)[a]	**4.03**	**4.55**	**4.60**	**c** (8.32–3.88)	**w**
Pyr(H10)–DMA(H14/H14′)[a]	**4.98**	(**3.52**)	**4.59**	**d** (8.33–7.28)	**w**
Pyr(H2)–DMA(H14/H14′)[a]	5.61	5.74	(**3.63**)	N/D[c]	N/D[c]
Pyr(H10)–DMA(H15/H15′)[a]	6.99	(4.28)	6.15	N/D[c]	N/D[c]
Pyr(H2)–DMA(H15/H15′) [a]	7.63	7.84	(**4.81**)	N/D[c]	N/D[c]
Pyr(H3)–DMA(H14/H14′)[a]	7.64	7.77	(**4.88**)	N/D[c]	N/D[c]
Pyr(H3)–DMA(H15/H15′)[a]	9.46	9.68	(**4.90**)	N/D[c]	N/D[c]

[a] The distance is measured for the centroid of indicated groups. [b] Relative intensities of observed NOESY cross-peaks were ranked as weak (w), medium (m) and strong (s) corresponding to $3.5 \leq r \leq 5.0$ Å, $2.5 \leq r \leq 3.5$ Å and $r < 2.0$ Å, respectively.[37] Peak intensities were classified relative to reference cross-peak **1** reflecting DMA(H14/H14′)-DMA(H15/H15′) intra-group interactions (2.42 Å). [c] Cross-peak was not detected in the NOESY spectrum.

of distances calculated for conformer **1b** show satisfactory correlation with the experimental data, there are two interactions (Pyr(H10)–DMA(H14/H14′) and Pyr(H10)–DMA(H15/H15′), shown in **bold** and parenthesis), which are inconsistent with the experimental data. The solution structure could be a combination of **1a** and **1b** conformers with a relatively low component arising from **1b** (the NOE intensity is sensitive to the squared concentration and thus very sensitive to the percent **1b** present). In contrast, structure **1c** showed very poor correlation with experimental observations (Table 5, the greatest discrepancies are shown in **bold** and parenthesis). For instance, based on ^{1}H–^{1}H distances calculated for **1c**, one would expect to observe medium cross-peak for Pyr(H2)–DMA(H14/H14′) interactions (3.52 Å), and weak cross-peaks for Pyr(H2)–DMA(H15/H15′, Pyr(H3)–/DMA(H14/H14′) and Pyr(H3)–DMA(H15/H15′) interactions (4.81, 4.88 and 4.90 Å, respectively). However, no cross-signals were detected for these interactions showing a low contribution from conformer **1c** for **1** under these experimental conditions. Again, this is in good agreement with the theoretically calculated populations.

Discussion

Intramolecular exciplexes **1** and **2** were used as model systems to reveal major factors affecting the exciplex fluorescence signal, and thus to approach the problem of highly quenched or absent exciplex emission of DNA-mounted exciplexes in aqueous solution. For both compounds, the broad, long wavelength emission band (around 475–571 nm for **1** and 493–586 nm for **2**) with the associated large Stokes shifts (ranging from 133–246 nm, shown in Table 1 and 2), taken with the rather small changes in the value of λ_{max} for excitation of this band (338–347 nm) support the interpretation of this as an exciplex emission across the full range of solvents studied. The gradual shift in λ_{max} to longer wavelength as the polarity of the solvent increases, is also consistent with the charge transfer nature of exciplex emission.[29] These are the first reported cases to our knowledge of intramolecular exciplex formation in solvents of very high dielectric constant (*e.g.* NMF) that have not required an additive, such as cyclodextrins,[31,32] metal ions[33] or polyanions such as chondroitins[34] nor the presence of special features such as hydrophobic cavities such as those found in cyclophanes[35] and biomacromolecules.

Conformational aspects of intramolecular exciplex emission

There is evidence of more than a single exciplex-emissive conformation for donor–linker–acceptor structures comparable to those of **1** and **2**. *Ab initio* calculations of β-(1-pyrenyl)ethyl 4-cyanobenzoate were consistent with two folded conformations leading to exciplex emission in binary solvents.[36] Supersonic jet fluorescence studies of **5** detected two isomeric conformers. One of these, described as an "open" conformer leads to exciplex formation and the other, a "closed" conformer, leads to charge transfer fluorescence, which is distinct from exciplex fluorescence.[37] It is not entirely explicit what conformation(s) corresponds to these open and closed species. A detailed analysis of the conformational effects of intramolecular rotations on donor and acceptor moieties has been provided for ω–(1-pyrenyl)-α, *N*,*N*-dimethylaminoalkanes.[15] Studying the influence of conformational rotations in the equivalent of **5** with pyrene and DMA replaced by anthracene and naphthalene, respectively, provided calculations that the lowest energy conformer was face-to-face (3.3 Å separation) with two gauche conformations in the linker trimethylene bridge.[38] These authors calculated that the face-to-face conformation was 2500 cm^{-1} more stable than the extended conformation (separation *ca.* 8.3 Å), but the calculations did not need to involve solvent as they were used in supersonic jet studies of the exciplex system.

An indirect manifestation of the conformational contribution to intramolecular exciplexes comes from comparison of the

energies of exciplex emission of corresponding pairs of intra and intermolecular exciplexes in various solvents. In intermolecular exciplexes it is generally assumed, in line with the situation for the pyrene excimer, that a face-to-face orientation of donor and acceptor will be achievable to a high approximation (unless some particular steric constraint is present). This will give maximal orbital overlap; it will be modified by the rotation of the faces relative to each other (governed by the substituent pattern on each of them), as well as by the differences in energy of the orbitals involved in potential overlap. For an intramolecular exciplex of structures comparable to **1**–**5**, perfect face-to-face orientation of donor and acceptor is energetically unrealisable. There is evidence that intramolecular exciplexes can emit from such non-perfect face-to-face states.[37,39] Lewis *et al.* reported[39] that published data[40,41] indicate that intramolecular exciplexes emit at 430 nm and intermolecular at 460 nm for pyrene–aniline systems, but the systems that had to be compared were not from a single study and from different laboratories. However, we found that the intramolecular exciplex from **1** emits at *ca.* 30 nm longer wavelength than the corresponding intermolecular exciplex of pyrene (1×10^{-5} M) and DMA (1×10^{-2} M), for example in toluene, EGDE, THF and DCM (Table 3). A similar effect (although less pronounced) was observed for intermolecular exciplexes formed by pyrene and substituted-DMAs (Table 3), showing 6–16 nm hypsochromic shifts of the exciplex band compared with that of **1**. Clearly, exciplex emission λ_{max} is not only influenced by mutual spatial orientation of the exci-partners, but it is also affected by many other factors. These include redox potential (which in turn is influenced by the nature of linker group/substitutions within intramolecular exciplexes) as well as energy of solvent re-organisation. Also, for intermolecular exciplexes a very high concentration of the signal silent partner (*e.g.* DMA) is required (10^{-2} M *cf.* 10^{-5} M for intermolecular and intramolecular exciplexes, respectively), which presumably affects the exciplex emission λ_{max}.

Previous study of intramolecular exciplexes[36] suggested possible correlation between efficiency of exciplex formation and ground state conformation of small organic molecules. In attempt to explain ability of **1** and **2** to emit as exciplexes in broad range of organic solvents, we evaluated structural properties of ground state conformations of **1** in chloroform using both ^{1}H NMR and molecular modelling.

Structural analysis of small flexible molecules ($M_r < 500$) is complicated by the fact that these molecules normally exist as conformational assemblies in solution, and are usually represented by families of rapidly equilibrating structures characterised by an averaged NMR spectrum. Also, quantitative ^{1}H–^{1}H distance measurements are rather problematic due to the fact that the calculated distance tends to be heavily weighted towards shorter separation since the NOE is very much more intense for these because of the r^{-6} dependency. Thus, in this study we performed qualitative evaluation of possible ground state conformation(s) of **1**, representing an average conformation(s) of a set of rapidly equilibrating conformers.

Molecular modelling calculations revealed three possible conformations for **1** (Fig. 5, Table 4). Structures **1a** and **1b** represent two major low-energy gauche-like conformations and are characterised by non-parallel orientation of the exci-partners. In low dielectric solvent, the distance between pyrene and DMA centroids was calculated as 8.36 and 7.63 Å for **1a** and **1b**, respectively. Minor conformer **1c** represents a folded structure with nearly parallel orientation of the exci-partners separated by only 5.06 Å.

Although conformer **1c** provides the most suitable mutual orientation of pyrenyl and DMA exci-partners in ground state, which is favourable for successful exciplex formation, the high E_{total} energy value (Table 4) suggests low probability of this conformation in solution. These data are supported by NMR structural studies of **1** in chloroform showing the absence of some important pyrene–DMA NOE interactions (*i.e.* Pyr(H2)–DMA(H14/H14′), Pyr(H2)–DMA(H15/H15′), Pyr(H3)–DMA(H14/H14′) and Pyr(H3)–DMA(H15/H15′) that one would expect to detect in NOESY spectrum of **1c** conformer. In contrast, structural parameters (^{1}H–^{1}H distances) calculated for the low-energy conformers **1a** and **1b** are in a good agreement with experimentally observed NOESY cross-peaks obtained for **1** in chloroform, suggesting that these structures are averaged representatives of two families of ground-state conformation, starting from which exciplex could be formed by internal rotations on photo-excitation.

An analogous effect was observed for **2** (data not presented). Similar NOE-interactions between pyrenyl and DMA exciplex partners (*i.e.* DMA(H14/H14′)–CH_2(11), Pyr(H2)–CH_2(13), Pyr(H10)–CH_2(13) and Pyr(H10)–DMA(H14/H14′) were detected in the NOESY spectrum of **1**, recorded in methanol-d_4, DMSO-d_6, acetonitrile-d_3 under identical conditions (from a manuscript in preparation). These observations indicate gauche-like ground-state conformations for **1** in a broad range of organic solvents, and we are analysing such data in terms of influence of molecular conformation on ability to form exciplexes in variety of solvents of different polarity.

Exciplexes formed by self-assembly of oligonucleotides

By attaching pyrenyl and dimethylaminoanilino or dimethylaminonaphthyl groups to oligonucleotides as in Scheme 1, the concept of a DNA-detector formed by an assembled exciplex can be introduced.[2] In this construct the pyrenyl group is attached to the 5′-terminus of a short (8-mer) oligonucleotide and the naphthaleno group to the 3′-end of a second short oligonucleotide (these are probe oligonucleotides for their complementary target DNA sequence). On hybridisation to the target the two probes align adjacent to one another and the exciplex-forming partners (pyrene and dialkylaminonaphthalene) become juxtaposed. The problem we faced with this was that in fully aqueous buffer the exciplex, if it formed at all, was not emissive. However, we found that by running the DNA systems in 80% *v*/*v* trifluoroethanol-containing buffer strong exciplex emission was possible.[1,2] It appears that this particular level of trifluoroethanol is critical and promotes the provision of a sufficiently hydrophobic solvent medium of lowered polarity to favour exciplex emission. It also is likely to favour a specific structural change of the DNA duplex that brings the exciplex-forming partners suitably close together for emission, and also probably balances the hydrophobic attraction of the pyrene and naphthalene rings to the DNA such that their mutual attraction in the excited state becomes possible. Our NMR studies of **1** and **2** provide ground-state evidence that such components can pre-associate and hence favour exciplex formation. Exciplex emission is not merely a matter of solvent polarity in the DNA case because of many solvents tested only a few were

able to induce exciplex emission.[1] The model studies reported here provide evidence that, given suitable structural and redox-potential characteristics, simple organic intramolecular exciplexes can emit even in media with extremely high dielectric constants.

Experimental

1-Pyrenylmethylamine and 4-dimethylaminobenzoyl chloride were purchased from Aldrich Chemical Co. Syntheses were monitored by thin layer chromatography on plastic sheets pre-coated to 0.2 mm with aluminium oxide (N/UV_{254}) (Merck, Darmstadt). Visualisation of spots for thin layer chromatography was performed using a UV GL-58 Mineral-Light lamp and/or by means of iodine vapour. Melting points were determined using a Köfler Melting Point apparatus microscope (Reichert, Austria).

Reverse phase HPLC analysis of **1** and **2** was performed using a HPLC Holochrome 302 (Gilson) chromatograph equipped with a C18 column (Vydac™, particle size 10 μm, inner diameter 10 mm, length 250 mm, pore size 300 Å). The sample was eluted using an increasing gradient of acetonitrile in water (0–80%) with fraction detection at 258 nm.

NMR spectra were recorded using a 5 mm QNP probehead on a 300 MHz Bruker Avance-300 spectrometer operating at 300 MHz for ^{1}H-NMR and 75 MHz for ^{13}C-NMR and using XWIN NMR system software. Chemical shifts (δ) are reported in parts per million (ppm) peak positions relative to Me_4Si (0.00 ppm) as internal reference. Data are reported according to the following convention: chemical shift, (integrated intensity, splitting patterns, assignment). Abbreviations used for splitting patterns are: s, singlet; d, doublet; t, triplet; q, quartet; p, pentet; m, unresolved multiplet.

Fast-atom bombardment mass spectra (FAB-MS) were taken in the Department of Chemistry, University of Manchester using a Kratos-Concept instrument operating in the FAB mode (Xe-beam bombardment) using m-nitrobenzyl alcohol (Aldrich Chemical Co.) as a matrix. Elemental analyses were recorded in the Department of Chemistry, University of Manchester, using an EA 1108-Elemental Analyzer (Carlo Erba Instruments).

Synthesis

N-(4-Dimethylaminobenzyl)-*N*-(1-pyrenemethyl)amine (**1**), isolated as the dihydrochloride salt, was synthesised by BH_3THF reduction of the amide (**3**) resulting from 1-pyrenylmethylamine and 4-dimethylaminobenzoyl chloride. *N′*-4-dimethylaminonaphthyl-*N*-(1-pyrenemethyl)amine (**2**) was synthesised in a similar manner from its amide (**4**).

***N*-(1-Pyrenemethyl)-4-(dimethylamino)benzamide (3).** A solution of 1-pyrenemethylamine hydrochloride (0.5 g, 1.865 mmol) in dichloromethane (150 ml) was treated with triethylamine (0.45 g, 4.47 mmol) and stirred for 30 min at room temperature. 4-Dimethylaminobenzoyl chloride (0.34 g, 1.865 mmol) in dichloromethane (50 ml) was added dropwise over 30 min and the mixture stirred for 5 h until TLC (CH_2Cl_2–EtOAc, 9 : 1 *v*/*v*) indicated completion of reaction. The reaction mixture was washed successively with 1 N HCl (1 × 100 ml), 1 N $NaHCO_3$ (3 × 100 ml), H_2O (100 ml) and brine (100 ml) and the organic layer dried over anhydrous Na_2SO_4. Evaporation of solvent afforded crude amide product (**3**), which was recrystallized from diethyl ether to give a white solid (0.358 g, 50.6%); mp, 204–206 °C. R_f: 0.09 (DCM), 0.53 (DCM : EtOAc, 2 : 1) $C_{26}H_{22}N_2O$ requires C 82.5%, H 5.9%, N 7.4%; found C 82.3%, H 5.8%, N 7.2%. Precise mass spectroscopy gave 379.1807 Daltons (calculated mass 379.1805). ^{1}H-NMR, (δ_H, $CDCl_3$): 2.98 (s, 6H, –N–C*H*$_3$); 5.34 (d, 2H, Py–C*H*$_2$–NH–); 6.34 (bt, 1H, –N*H*CO–); 6.61(d, 2H, –Ar); 7.68 (d, 2H, –Ar); 8.01–8.24 (m, 9H, –Pyr), ^{13}C-NMR (δ_C, $CDCl_3$): 40.1; 42.5; 106.5, 111.0; 120.8, 123.0; 124.7; 124.8; 125.0; 125.3, 126.1; 127.4; 127.5; 128.2, 128.5; 129.2; 130.8; 131.2, 131.24; 131.5, 131.6, 149.3, 152.4, 154.3, 156.8, 167.1.

***N*-(1-Pyrenemethyl)-4-(dimethylamino)benzylamine (1).** To a solution of *N*-(1-pyrenemethyl)-4-(dimethylamino)benzamide (**3**, 0.3 g, 0.79 mmol) in dry THF (8 ml) was added borane (2.8 ml of 1 M in THF) at 0 °C over 10 min The clear solution was then refluxed under argon for 6 h. The flask was cooled to room temperature and sufficient 6 M hydrochloric acid (*ca.* 4 ml) slowly added to destroy excess borane and the amine–borane complex. The solution was stirred for 15 min at room temperature to allow complete hydrolysis of the amine–borane complex. THF was removed by rotary evaporator and the aqueous phase was saturated with sodium hydroxide pellets to form a yellow organic layer, which was extracted with chloroform (3 × 30 ml). The extracts were combined and dried over anhydrous sodium sulfate. The solvent was removed by rotary evaporator under reduced pressure and the residue purified by column chromatography on silica gel with CH_2Cl_2–EtOAc (1 : 1) as eluent. Evaporation of the solvent gave the pure product (**1**) as a light brown oil (0.25 g, 80%). The oil was dissolved in CH_2Cl_2–diethyl ether and hydrogen chloride gas bubbled through to form the dihydrochloride salt of **1** (which has better storage stability than free base) as a white solid, mp 247–253 °C (dec.); $C_{26}H_{26}N_2Cl_2{\cdot}0.5H_2O$ requires C 70.0%, H 6.1%, N 6.3%, Cl 15.9%; found C 70.4%, H 6.3%, N 6.1%, Cl 15.7%. *N*-(1-Pyrenemethyl)-4-(dimethylamino)benzylamine (**1**) gave a single peak on reversed phase HPLC (Vydac 10 μm C18 250 × 10 mm column, 0–80% CH_3CN–H_2O, 6 mL min^{-1}, detection at 258 nm). TLC R_f 0.58 [CH_2Cl_2 (3 ml): 35% NH_4OH (2 drops)]. Precise mass spectroscopy gave 364.1934 Daltons (calculated mass 364.1939). ^{1}H-NMR (300 MHz, δ_H, $CDCl_3$, free amine form; assignments using NOESY and COSY): 1.74* (bs, 1H, –N*H*(12)); 2.94 (s, 6H, 2-NC*H*$_3$(17)); 3.87 (sharp m, 2H, –NC*H*$_2$(13)–Ar); 4.49 (s, 2H, –NC*H*$_2$(11)–Pyr); 6.75–6.72 (dd, 2H, H15′/H15″–Ar); 7.25–7.28 (dd, 2H, H14′/H14″ –Ar); 7.97–8.00 (d, 1H, –Pyr(*H2*)), 7.90–8.20; (m, 7H, –Pyr), 8.33–8.36 (d, 1H, –Pyr(*H10*)), ^{13}C NMR (δ_C, $CDCl_3$, free amine): 41.2, 51.3, 53.7, 113.2, 123.8, 125.1, 125.4, 125.4, 125.5, 126.2, 127.1, 127.4, 127.5, 127.9, 128.2, 128.8, 129.0, 129.6, 129.7, 131.0, 131.3, 131.8, 134.6, 150.3.

***N*-(1-Pyrenylmethyl)-4-(dimethylamino)naphthalene-1-carboxamide (4).** A solution of 1-pyrenemethylamine hydrochloride (0.2 g, 0.72 mmol) in CH_2Cl_2 (20 ml) was treated with triethylamine (0.11 ml, 0.79 mmol) and stirred for 30 min at room temperature. 4-Dimethylaminonaphthalene-1-carboxylic acid (0.194 g, 0.76 mmol, Lancaster Chemicals, UK) in CH_2Cl_2 (20 ml) and 4-dimethylaminopyridine (0.088 g, 0.72 mmol) were added. To this solution, *N*,*N*-diisopropylcarbodiimide (0.12 ml, 0.77 mmol) was added dropwise at 0 °C under nitrogen and the reaction mixture refluxed for 3 h. The mixture was stirred overnight at room temperature under drying tube and then washed with 1 N $NaHCO_3$ (50 ml) and H_2O (2 × 50 ml). The

organic layer was dried over anhydrous $MgSO_4$. Evaporation of solvent gave crude **4** and column chromatography on silica gel with CH_2Cl_2–hexane (19 : 1) afforded the pure product **4** as a white solid (87%), mp 185–188 °C. $C_{30}H_{24}N_2O$ requires C 84.1%, H 5.7%, N 6.5%; found C 84.5%, H 5.6%, N 6.4%. Precise mass spectroscopy gave 429.1959 Daltons (calculated mass 429.1961). ^{1}H-NMR (δ_H, $CDCl_3$): 2.86 (s, 6H, 2-N–CH_3); 5.45 (d, 2H, Py–CH_2–NH–); 6.30 (bt, 1H, –NH–CO); 6.87–6.90 (m, 1H, –Ar); 7.47–7.55 (m, 3H, –Ar); 8.01–8.25 (m, 9H, –Ar); 8.44–8.50 (dd, 2H, –Ar). ^{13}C NMR (δ_C, $CDCl_3$): 42.5, 44.9, 112.1, 123.0, 124.6, 124.8, 125.4, 125.45, 124.5, 124.6, 126.1, 127.0, 127.3, 127.4, 127.6, 128.3, 128.4, 128.6, 129.2, 130.8, 131.1, 131.2, 131.3, 131.8, 132.8, 134.1, 147.5, 153.3, 169.4.

***N*-(1-Pyrenemethyl)-4-(dimethylamino)naphthalene-1-yl amine (2).** *N*-(1-Pyrenylmethyl)-4-(dimethylamino)naphthalene-1-yl amine (**2**), prepared from *N*-(1-pyrenylmethyl)-4-(dimethylamino)naphthalene-1-carboxamide (4, 0.22 g, 0.5 mmol) by borane reduction in dry THF (7 ml) as described above, was a brown oil which was purified by column chromatography on silica gel with CH_2Cl_2–EtOAc (2 : 1). Evaporation of the solvent gave pure 2 as a brown oil (0.15 g, 70%), which was converted to the dihydrochloride salt. $C_{30}H_{26}N_2{\cdot}2HCl{\cdot}2H_2O$ requires C 69.1%, H 5.8%, N 5.4%, Cl 13.6%; found C 69.1%, H 6.2%, N 5.2%, Cl 13.5%. m/z (ES$^+$) 1243 (3M$^+$-1, 5%), 829 (2M$^+$-1, 100%), 415 (M$^+$-1, 25%), 184 (M$^+$–$C_{17}H_{12}N$, 69%). R_f 0.14 (CH_2Cl_2–EtOAc, 20 : 1). ^{1}H-NMR (δ_H,$CDCl_3$): 1.32 (bs, 2H, –NH_2); 3.11 (t, 2H, NpCH_2); 3.20 (t, 2H, Pyr–CH_2NH); 7.49–7.66 (m, 5H, –Ar); 7.80 (d, 1H, –Ar); 8.06 (d, 1H, –Ar); 8.72–8.59 (dd, 2H, –Ar).

UV-visible absorption spectra

All UV-visible spectra were measured at 20 °C on a Cary-Varian 1E UV-Visible spectrophotometer equipped with a Peltier-thermostatted cuvette holder. The Cary WinUV (version 3) software suite was used for all measurements. The wavelength range used was 190–900 nm.

Fluorescence excitation and emission spectra

All fluorescence spectra were recorded at 20 °C on a Shimadzu RF-5301PC spectrofluorophotometer (Shimadzu Corporation, Kyoto, Japan) fitted with a single non-constant temperature-stirred cell holder and equipped with a 150 W Xenon lamp, a blazed holographic concave diffraction grating monochromator (F/2.5 for both excitation and emission sides), and a photomultiplier tube detector for operation in the 220–900 nm scan range. Wavelength accuracy was ±1.5 nm. For comparative purposes a standard concentration of tested small molecules in the 1 cm-square cuvette was 1×10^{-5} M. Excitation wavelengths for both monomer and exciplex emission were optimised for each solvent (see Table 1). In most cases excitation slit width was 3 nm both for excitation and emission spectra unless indicated otherwise. The "Automatic shutter-on" regime was used to minimise photo-degradation of compounds in the cuvette.

Calculation of areas under the corrected emission curve

The efficiency of exciplex formation was evaluated using areas under the fluorescence emission curve of exciplex and monomer bands. AUC^M and AUC^E are the fractional areas under the corrected emission curve for monomer and exciplex fluorescence band, respectively, normalised relative to the total integral emission AUC^Σ, where $AUC^\Sigma = AUC^M + AUC^E$, and $AUC^\Sigma = 1$. AUC^M and AUC^E were calculated using experimentally measured areas under the fluorescence emission curve of monomer band (S^M) and exciplex band (S^E), respectively: $AUC^M = S^M/(S^M + S^E)$, whereas $AUC^E = S^E/(S^M + S^E)$. To determine S^M and S^E, emission spectra were converted from wavelength to frequency using Microsoft Office Excel 2003. The area under the curve for exciplex band (S^E) and locally excited state band (S^M) was determined by numerical integration using Simpson's method, approximating the area of each portion of the curve defined by adjacent data points; S was calculated as the sum of individual segments:

$$S = \Sigma\,[(y_i + 4y_{i+1} + y_{i+2})/6 \times (x_{i+1} - x_i)] \quad (1)$$

Determination of relative quantum yields

The relative quantum yields for **1** and **2** were measured in toluene, diethyl ether, ethyl acetate, THF and ethylene glycol dimethyl ether, using Hoechst 33258 as the reference standard (reported quantum yield value of Hoechst 33258 in ethanol is 0.5[42]). The relative quantum yields of the exciplex band of **1** and **2** were determined using eqn (2)[43]:

$$\Phi_{(SM)} = (A_{st}/A_{SM}){\cdot}(F_{SM}/F_{St}){\cdot}(n_{SM}/n_{St})^2{\cdot}\Phi_{st} \quad (2)$$

where Φ is the fluorescence quantum yield, A is the absorption intensity at the excitation wavelength, F is the area under the corrected emission curve and n is the refractive index for the solvent used for the quantum yield measurement. Subscripts $_{SM}$ and $_{St}$ refer to the respective variables of sample (**1** or **2**) and standard (Hoechst 33258), respectively.

The excitation wavelengths used for the measurements of fluorescence emission of **1**, **2** and Hoechst 33258 were optimised for each solvent, and normally corresponded to λ_{max} for excitation of the pyrene LES (λ^M_{max}), presented in Tables 1 and 2. In each experiment absorption intensities of both tested compound (**1** or **2**) and standard were measured at a wavelength corresponding to the optimised excitation wavelength. Two series of absorption and fluorescence measurements were performed for Hoechst 33258 using 1 and 2 μM dye concentrations to ensure a linear response of absorbance/fluorescence with concentration. The working concentrations of **1** and **2** in the cuvette varied from 2 to 0.625 μM, which were shown in independent experiments to be within this region of linear response of absorbance/fluorescence with concentration.

NMR spectroscopy for conformational analysis

1D ^{1}H NMR spectra were collected into 65 K data points over a spectral width of 6 kHz, with a relaxation delay of 1 s between scans. Standard XWIN-NMR programs were used to accumulate phase-sensitive NOESY spectra with mixing times τ_{mix} of 0.300, 0.500, 0.700, 0.800, 1.00 and 1.500 s. Data were acquired over 3 kHz spectral width for **1** (15 mM) in $CDCl_3$, methanol-d_4, DMSO-d_6 and acetonitrile-d_3 at 17 °C. Spectra were collected with quadrature detection, and the size of data matrix ($t_1 \times t_2$)

was 256 × 2048. 16 transitions were acquired per t_1 increment with a 2 s relaxation delay between transitions.

Computational methods

Conformational analysis of **1** was performed theoretically using an internal coordinate, random search *via* the Monte Carlo/multiple minimum (MC/MM) approach, to identify the lowest energy conformation in solution.[44] The solute was described using the all-atom MMFF potential,[45] including a modification to maintain planarity at the aromatic nitrogen.[46] The effect of solvent was incorporated into MC/MM calculations using parametrizations of the generalised Born/surface area (GB/SA) continuum solvent model for chloroform to represent low dielectric media ($\varepsilon = 5$) and water[47] to model a high dielectric environment ($\varepsilon = 80$). Cut-offs of 12.0 and 7.0 Å were employed for electrostatic and van der Waals non-bonded interactions, respectively. Each of the two MC simulations involved 10^4 steps at 300 K, applied to all rotatable bonds, with random torsional rotations of up to ±180°. This was combined with 10^3 steps of energy minimization. Conformations of interest obtained from the MC/MM approach were then subjected to exhaustive re-optimization, also in the presence of reaction field solvent. The stability of these conformations is reported as the total potential energy relative to the MC/MM global minimum structure. All conformational analysis calculations were performed using the MacroModel 8.0 and BatchMin suite of programs.[48]

Acknowledgements

We are grateful to the BBSRC and DTI for LINK and Follow-On awards, the Wolfson Foundation for financial support, and to Professor Gareth Morris for invaluable discussions on NMR spectroscopy.

References

1 E. V. Bichenkova, H. E. Savage, A. R. Sardarian and K. T. Douglas, *Biochem. Biophys. Res. Commun.*, 2005, **332**, 956–964.
2 E. V. Bichenkova, A. Sardarian, H. E. Savage, C. Rogert and K. T. Douglas, *Assay Drug Dev. Technol.*, 2005, **3**, 39–46.
3 K. Ebata, M. Masuko, H. Ohtani and M. Jibu, *Nucleic Acids Symp. Ser.*, 1995, **34**, 187–188.
4 K. Ebata, M. Masuko, H. Ohtani and M. Kashiwasake-Jibu, *Photochem. Photobiol.*, 1995, **62**, 836–839.
5 M. Masuko, H. Ohtani, K. Ebata and A. Shimadzu, *Nucleic Acids Res.*, 1998, **26**, 5409–5416.
6 M. Masuko, K. Ebata and H. Ohtani, *Nucleic Acids Symp. Ser.*, 1996, **35**, 165–166.
7 P. L. Paris, J. M. Langenhan and E. T. Kool, *Nucleic Acids Res.*, 1998, **26**, 3789–3793.
8 H. Rau and F. Totter, *J. Photochem. Photobiol., A*, 1992, **63**, 337–347.
9 H. Knibbe, *J. Chem. Phys.*, 1967, **47**, 1184–1185.
10 M. Gordon and W. R. Ware, *The Exciplex*, Academic Press Inc., 1975.
11 J. B. Birks, *Organic Molecular Photophysics*, Wiley, London, 1973, vol. 1.
12 S. Masaki, T. Okada, N. Mataga, Y. Sakata and S. Misumi, *Bull. Chem. Soc. Jpn.*, 1976, **49**, 1277–1283.
13 A. M. Swinnen, M. Van der Auweraer and F. C. De Schryver, *J. Photochem.*, 1985, **28**, 315–327.
14 Ph. Van Haver, N. Helsen, S. Depaemelaere, M. Van der Auweraer and F. C. De Schryver, *J. Am. Chem. Soc.*, 1991, **113**, 6849–6857.
15 A. M. Swinnen, M. Van der Auweraer, F. C. De Schryver, K. Nakatami, T. Okada and N. Mataga, *J. Am. Chem. Soc.*, 1987, **109**, 321–330.
16 T. Okada, T. Saito, N. Mataga, Y. Sakata and S. Misumi, *Bull. Chem. Soc. Jpn.*, 1977, **50**, 331–336.
17 T. Okada, T. Fujita, M. Kubota, S. Masaki and N. Mataga, *Chem. Phys. Lett.*, 1972, **14**, 563–568.
18 N. Mataga, *Pure Appl. Chem.*, 1984, **56**, 1255–1268.
19 J. W. Verhoeven, T. Scherer and R. J. Willemse, *Pure Appl. Chem.*, 1993, **65**, 1717–1722.
20 J. W. Verhoeven, *Pure Appl. Chem.*, 1990, **62**, 1585–1596.
21 M. Van der Auweraer, L. Viaene, Ph. Van Haver and F. C. De Schryver, *J. Phys. Chem.*, 1993, **97**, 7178–7184.
22 B. Wegewijs, R. M. Hermant, J. W. Verhoeven, A. G. M. Kunst and R. P. H. Rettschnick, *Chem. Phys. Lett.*, 1987, **140**, 587–590.
23 N. Orbach and M. Ottolenghi, *Chem. Phys. Lett.*, 1975, **35**, 175–180.
24 F. D. Lewis and B. E. Cohen, *J. Phys. Chem.*, 1994, **98**, 10591–10597.
25 U. Werner and H. Staerk, *J. Phys. Chem.*, 1995, **99**, 248–254.
26 J. Kypr, J. Chladkova, M. Zimulova and M. Vorlickova, *Nucleic Acids Res.*, 1999, **27**, 3466–3473.
27 E. V. Bichenkova, D. Marks, M. I. Dobrikov, V. V. Vlassov, G. A. Morris and K. T. Douglas, *J. Biomol. Struct. Dyn.*, 1999, **17**, 193–211.
28 E. V. Bichenkova, D. S. Marks, S. G. Lokhov, M. I. Dobrikov, V. V. Vlassov and K. T. Douglas, *J. Biomol. Struct. Dyn.*, 1997, **15**, 307–320.
29 J. B. Birks, *Photophysics of Aromatic Molecules*, Wiley, London, 1970.
30 T. Claridge, *High-Resolution NMR Techniques in Organic Chemistry*, Pergamon, Oxford, 2000.
31 G. S. Cox, N. J. Turro, N.-C. Yang and M.-J. Chen, *J. Am. Chem. Soc.*, 1984, **106**, 422–424.
32 N. J. Turro, T. Okubo and G. C. Weed, *Photochem. Photobiol.*, 1982, **35**, 325–329.
33 A. Bencini, A. Bianchi, A. Masotti, B. Valtancoli, C. Lodeiro, A. J. Parola, F. Pina and J. S. de Melo, *Chem. Commun.*, 2000, 1639–1640.
34 M. K. Pal and J. K. Ghosh, *J. Photochem. Photobiol., A*, 1994, **78**, 31–37.
35 D. R. Benson and J. Fu, *Tetrahedron Lett.*, 1996, **37**, 4833–4836.
36 J. Kawakami, J. Nakamura and M. Iwamura, *J. Photochem. Photobiol., A*, 2001, **140**, 199–206.
37 M. Kurono and M. Itoh, *J. Phys. Chem.*, 1995, **99**, 17113–17117.
38 X. Wang, D. H. Levy, M. B. Rubin and S. Speiser, *J. Phys. Chem. A*, 2000, **104**, 6558–6565.
39 F. D. Lewis, J. M. Wagner-Brennan and A. M. Miller, *Can. J. Chem.*, 1999, **77**, 595–604.
40 S. Basu, *J. Photochem.*, 1978, **9**, 539–544.
41 N. C. Yang, D. W. Minsek, D. G. Johnson, J. R. Larson, J. W. Petrich, R. Gerald, III and M. R. Wasielewski, *Tetrahedron*, 1989, **45**, 4669–4681.
42 H. Gorner, *Photochem. Photobiol.*, 2001, **73**, 339–348.
43 S. Fery-Forgues and D. Lavabre, *J. Chem. Educ.*, 1999, **76**, 1260–1264.
44 G. Chang, W. C. Guida and W. C. Still, *J. Am. Chem. Soc.*, 1989, **111**, 4379–4386.
45 T. A. Halgren, *J. Comput. Chem.*, 1996, **17**, 490–519.
46 T. A. Halgren, *J. Comput. Chem.*, 1999, **20**, 720–729.
47 W. C. Still, A. Tempczyk, R. C. Hawley and T. Hendrickson, *J. Am. Chem. Soc.*, 1990, **112**, 6127–6129.
48 F. Mohamadi, N. G. J. Richards, W. C. Guida, R. Liskamp, M. Lipton, C. Caufield, G. Chang, T. Hendrickson and W. C. Still, *J. Comput. Chem.*, 1990, **11**, 440–467.

